Published in final edited form as:
Atherosclerosis. 2016 January ; 244: 9–21. doi:10.1016/j.atherosclerosis.2015.10.109.

Monoglyceride lipase deficiency modulates endocannabinoid signaling and improves plaque stability in ApoE-knockout mice

Nemanja Vujic[a], **Stefanie Schlager**[a], **Thomas O. Eichmann**[b], **Corina T. Madreiter-Sokolowski**[a], **Madeleine Goeritzer**[a], **Silvia Rainer**[a], **Silvia Schauer**[c], **Angelika Rosenberger**[d], **Albert Woelfler**[d], **Prakash Doddapattar**[a,1], **Robert Zimmermann**[b], **Gerald Hoefler**[c], **Achim Lass**[b], **Wolfgang F. Graier**[a], **Branislav Radovic**[a], and **Dagmar Kratky**[a,*]

[a]Institute of Molecular Biology and Biochemistry, Medical University of Graz, Graz, Austria

[b]Institute of Molecular Biosciences, University of Graz, Graz, Austria

[c]Institute of Pathology, Medical University of Graz, Graz, Austria

[d]Division of Hematology, Medical University of Graz, Graz, Austria

Abstract

Background and aims—Monoglyceride lipase (MGL) catalyzes the final step of lipolysis by degrading monoglyceride (MG) to glycerol and fatty acid. MGL also hydrolyzes and thereby deactivates 2-arachidonoyl glycerol (2-AG), the most abundant endocannabinoid in the mammalian system. 2-AG acts as full agonist on cannabinoid receptor type 1 (CB1R) and CB2R, which are mainly expressed in brain and immune cells, respectively. Thus, we speculated that in the absence of MGL, increased 2-AG concentrations mediate CB2R signaling in immune cells to modulate inflammatory responses, thereby affecting the development of atherosclerosis.

Methods and results—We generated apolipoprotein E (ApoE)/MGL double-knockout (DKO) mice and challenged them with Western-type diet for 9 weeks. Despite systemically increased 2-AG concentrations in DKO mice, CB2R-mediated signaling remains fully functional, arguing against CB2R desensitization. We found increased plaque formation in both *en face* aortae (1.3-fold, $p = 0.028$) and aortic valve sections (1.5-fold, $p = 0.0010$) in DKO mice. Interestingly, DKO mice also presented reduced lipid (12%, $p = 0.031$) and macrophage content (18%, $p = 0.061$), elevated intraplaque smooth muscle staining (1.4-fold, $p = 0.016$) and thicker fibrous caps (1.8-fold, $p = 0.0032$), together with a higher ratio of collagen to necrotic core area (2.5-fold, $p = 0.0003$) and expanded collagen content (1.6-fold, $p = 0.0007$), which suggest formation of less vulnerable atherosclerotic plaques. Treatment with a CB2R inverse agonist prevents these effects in DKO mice, demonstrating that the observed plaque phenotype in DKO mice originates from CB2R activation.

*Corresponding author. Institute of Molecular Biology and Biochemistry, Medical University of Graz, Harrachgasse 21, 8010 Graz, Austria. dagmar.kratky@medunigraz.at (D. Kratky).
[1]Present address: Department of Internal Medicine, University of Iowa, Iowa City, USA.

Appendix A. Supplementary data
Supplementary data related to this article can be found at http://dx.doi.org/10.1016/j.atherosclerosis.2015.10.109.

Conclusion—Loss of MGL modulates endocannabinoid signaling in CB2R-expressing cells, which concomitantly affects the pathogenesis of atherosclerosis. We conclude that despite larger lesion size loss of MGL improves atherosclerotic plaque stability. Thus, pharmacological MGL inhibition may be a novel intervention to reduce plaque rupture.

Keywords

Apolipoprotein E-deficient mice; Atherosclerosis; Cannabinoid 2 receptor; Endocannabinoid signaling; 2-Arachidonoyl glycerol

1. Introduction

Intracellular lipolysis requires three consecutive steps, mediated by adipose triglyceride lipase, hormone-sensitive lipase, and monoglyceride lipase (MGL) [1]. Thus, MGL catalyzes the final step in triglyceride (TG) hydrolysis by cleaving monoglyceride (MG) to glycerol and fatty acid. In addition to MGL, at least four other enzymes are capable of hydrolyzing MGs: hormone-sensitive lipase [2], fatty acid amide hydrolase [3], and α/β hydrolase domain-containing 6 and 12 [4].

Among the MG substrates hydrolyzed by MGL is 2-arachidonoyl glycerol (2-AG), the most abundant endocannabinoid (EC) in mammals. 2-AG acts as full agonist on cannabinoid receptor type 1 (CB1R) [5] and CB2R [6] and several of its effects are mimicked by Δ^9-tetrahydrocannabinol (THC), the psychoactive component of *Cannabis sativa*. CB1R is predominantly expressed in brain, whereas lower receptor densities are found in liver, pancreas, adipose tissue, and skeletal muscle. Its activation is associated with increased food intake [7], lipogenesis, non-adipose tissue steatosis [8], insulin resistance [9], and thrombogenesis. CB1R inhibition results in reduced oxidative stress and improved endothelial function [10] as well as reduced atherosclerosis in LDL receptor-deficient (−/−) mice [11]. Thus, CB1R activation promotes the development of the metabolic syndrome and concomitantly atherosclerosis development. In contrast, CB2R is highly expressed in immune cells and the signaling mediated by this receptor leads to impaired antigen presentation [12,13], lymphocyte and macrophage migration [14,15], modulation of cytokine and chemokine production (reviewed in [16]), and induction of apoptosis [17,18]. These effects diminish critical functions of the immune system and therefore presumably attenuate atherosclerosis-associated inflammatory responses. Indeed, CB2R blockade was shown to aggravate atherogenesis [19,20] and CB2R activation to attenuate pro-inflammatory responses [21] and atherosclerosis development [15,20,21]. Low doses of THC reduced atherosclerotic lesion size in apolipoprotein E (ApoE)−/− mice by decreasing macrophage migratory capacity, which resulted in reduced lesional macrophage content [15]. These beneficial effects were abolished when mice were treated with a specific CB2R antagonist, suggesting that CB2R but not CB1R signaling is crucial for the anti-atherosclerotic effect of THC [15]. In contrast, increased 2-AG production in plaques of ApoE−/− mice together with elevated *in vitro* chemotaxis of macrophages toward 2-AG argue against an atheroprotective role of 2-AG in atherosclerosis [22]. Thus, a clear picture of the *in vivo* effects of 2-AG on atherosclerotic plaque formation is still missing.

Europe PMC Funders Author Manuscripts

Although MGL was discovered simultaneously with hormone-sensitive lipase in 1964 [23], MGL−/− mice have been generated only recently [24-26]. MGL deficiency in mice impairs lipolysis and attenuates diet-induced insulin resistance [26]. Defective degradation of 2-AG, however, does not provoke cannabinomimetic effects on feeding behavior, lipogenesis, and energy expenditure due to downregulation and blunting of CB1R-mediated signaling (desensitization) [24-26].

MGL directly affects lipolysis and indirectly influences energy metabolism, lipid homeostasis, and immune responses by degrading 2-AG and modulating the EC system. We therefore hypothesized that in the absence of MGL, increased 2-AG concentrations may act on CB2R, thereby modulating immune responses and atherogenesis. Despite increased atherosclerotic lesion formation in ApoE/MGL double-knockout (DKO) compared to ApoE −/− mice, plaques from DKO mice have reduced lipid and macrophage content, markedly increased amount of collagen, and a thicker fibrous cap, demonstrating lesion stabilization. These effects in DKO mice were reversed by *in vivo* CB2R antagonism, indicating that the atherosclerotic phenotype of DKO mice is mediated via CB2R activation.

2. Materials and methods

Full details are presented in the Online Supplement materials.

2.1. Animals and diets

ApoE−/−MGL−/− (DKO) mice were generated by crossing ApoE−/− (The Jackson Laboratory, Bar Harbor, ME) with MGL−/− mice [26]. At the age of 6–8 weeks, female mice were challenged with Western-type diet (WTD, 21% fat, 0.2% cholesterol; Ssniff Spezialdiaeten GmbH, Soest, Germany) for 9 weeks to induce atherosclerotic plaque formation. Where indicated, mice were treated daily with the CB2R inverse agonist SR144528 (Cayman Chemical, Ann Arbor, MI) during the last three weeks of WTD feeding by gastric gavage. All protocols were approved by the Austrian Federal Ministry of Science, Research and Economy, Vienna, Austria.

2.2. Quantification of 2-AG in plasma, aorta, and macrophages

Two hundred µl plasma were mixed with 800 µl dH_2O. Aortae were homogenized in 800 µl dH_2O. Eight hundred µl of macrophage lysate was used for the extraction. Lipids were extracted twice with 4 ml $CHCl_3$:MeOH:H_2O (2:1:0.6, v:v:v) containing 2 µg C17:0 MG (Avanti Lipids, Alabaster, AL) as internal standard. MGs were isolated by solid phase extraction using a self-packed silica gel column. Fractions were obtained by eluting lipids with 99:1 and 90:10 $CHCl_3$:MeOH (v:v) consecutively. 2-AG concentrations were quantitated in the latter fraction using an AQUITY-UPLC (Waters, Manchester, UK) equipped with a BEH-C18-column (2.1 × 150 mm, 1.7 µm; Waters), coupled to a SYNAPT™ G1 qTOF HD mass spectrometer (Waters) equipped with an ESI source [27].

2.3. Complete blood cell count and immunophenotyping of bone marrow

Complete blood cell count was performed with the Cell Counter Analyzer MS9-5V (Melet Schloesing Laboratories GmbH, Maria Enzersdorf, Austria).

Washed cell pellets from bone marrow were resuspended in 200 µl antibody cocktail and incubated at RT for 10 min, washed in buffer, and subsequently analyzed by flow cytometry.

2.4. White blood cell (WBC) half-life

Mice were injected with 3 mg EZ-Link Sulfo-NHS-Biotin (Pierce Biotechnology, Rockford, IL) into the tail vein. At indicated time points, blood was drawn from *vena facialis*. Red blood cells were lysed with ammonium–chloride–potassium lysis buffer. Remaining WBCs were washed with PBS/EDTA (400 × *g*, 5 min, 4 °C). Cells were fixed with 10% neutral buffered formalin (methanol-free) for 10 min at 4 °C, washed once with PBS/EDTA, and stained with Streptavidin-PE antibody (eBioscience, San Diego, CA) in PBS containing 3% FCS (20 min, 4 °C). Data were acquired on a FACSCalibur (BD Biosciences, San Jose, CA) and the analysis was performed using Flowjo (Treestar Inc, San Carlos, CA). The frequencies of specific cell types were calculated as the percentage of living cells.

2.5. MG hydrolase activity assay

MG hydrolase activity was determined as described [26].

2.6. Cytosolic Ca^{2+} imaging using Fura-2/AM

Ca^{2+} imaging was performed as described [28].

2.7. In vivo macrophage phagocytosis assay

Mice were i.p. injected with 200 µl fluorescein-labeled *Escherichia coli* BioParticles® (Molecular Probes®, Life Technologies, Carlsbad, CA) suspended in HBSS. *In vivo* phagocytosis after 2 h of injection was determined as previously described [29].

2.8. Preparation of histological sections and atheroassays

Anesthetized mice were perfused with PBS/EDTA for 10–15 min. The abdominal part of the aorta was removed and frozen in liquid N_2 for RNA isolation. Animals were perfused with 10% neutral buffered formalin (methanol-free) for 15 min. The upper part of the aorta was excised from the thoracic cavity and stored in formalin until staining. Upper two thirds of the heart were fixed with formalin for 24 h and stored in 30% sucrose. One day before sectioning, hearts were transferred into Neg-50™ frozen section medium (Richard-Allan Scientific, Kalamazoo, MI). Serial sections (7–8 mm) of aortic root were cut at −20 °C using a cryostat-microtome (HM 560 Cryo-Star; Microm International GmbH, Walldorf, Germany).

Mean lesion area (mm^2) was calculated from 14 to 15 consecutive Oil red O-stained sections per mouse. Sections were stained immunohistochemically for the presence of macrophages, collagen, smooth muscle cells, caspase 3, and CD31. For *en face* analysis, aortae were dissected and plaques were stained with Oil red O as described [30].

2.9. Statistics

Statistical analyses were performed using GraphPad Prism 5.0 software. Statistically significant differences were determined by Student's unpaired *t*-test and Welch correction

(in case of unequal variances) for two group comparison and ANOVA followed by Bonferroni correction for multiple group comparison. Data represent mean values ± SD. Values of $p < 0.05$ were considered significantly different.

3. Results

3.1. DKO mice exhibit increased plasma 2-AG concentrations

Challenging of ApoE−/− and DKO mice with WTD for 9 weeks resulted in comparable body weight gain (Fig. 1A) and food intake (ApoE−/−: 2.48 ± 0.37 g vs DKO: 2.75 ± 0.43 g, Fig. 1B). After 12 h of fasting, plasma TG, total cholesterol (TC), free cholesterol (FC), and cholesterol ester (CE) concentrations were comparable in both genotypes either fed standard chow or Western-type diet (WTD) (Table 1). Fast protein liquid chromatography revealed identical fasting plasma lipoprotein profiles for TG (Supplementary Fig. S1A) and TC concentrations (Supplementary Fig. S1B) between ApoE−/− and DKO mice after WTD feeding. In plasma of DKO animals, we measured 0.3 nmol/ml 2-AG (Fig. 1C), whereas in ApoE−/− mice plasma 2-AG concentrations were below the detection limit. Interleukin 6 (IL-6) plasma levels were at comparable and low levels in both genotypes, whereas monocyte chemoattractant protein 1 (MCP-1) concentrations were reduced in DKO mice (Supplementary Fig. S1C). These data indicate that MGL deficiency on the ApoE−/− background results in systemic accumulation of 2-AG.

3.2. Increased number of circulating white blood cells (WBCs) in DKO mice

Since EC signaling can influence immune responses and leukocyte function, we determined WBC counts in ApoE−/− and DKO mice after 9 weeks of WTD feeding. The total number of WBCs was increased in DKO mice (ApoE−/−: $7.91 \pm 1.07 \times 10^3$ vs DKO: $10.0 \pm 1.10 \times 10^3$ cells/μl, $p = 0.0016$) due to higher levels of lymphocytes, monocytes, and basophils, whereas the numbers of neutrophils and eosinophils were unaltered (Fig. 2A). An increased relative abundance of hematopoietic $Lin^-Sca\text{-}1^+c\text{-}Kit^+$ (LSK) cells in the bone marrow of DKO mice (ApoE−/−: 0.17 ± 0.03 vs DKO: 0.26 ± 0.08%, $p = 0.039$, Fig. 2B) and prolonged WBC half-life (Fig. 2C) were contributing factors to elevated circulating WBC numbers in DKO animals.

3.3. EC signaling is intact in DKO macrophages

Macrophages originate from monocytes and represent the most dominant cell type in the atheroma. Thus, we explored consequences of MGL deficiency in these cells. We found comparable expression levels of lipases, enzymes capable to degrade MGs and generate 2-AG, and Cb2r (Fig. 3A). Cb1r transcript was absent in macrophages from both genotypes. MG hydrolase activity was markedly reduced in DKO (0.28 ± 0.01 μmol/mg*h) compared to ApoE−/− macrophages (0.50 ± 0.04, $p = 0.0016$) (Fig. 3B). Accordingly, macrophage 2-AG concentrations were significantly increased in DKO (63.19 ± 22.96 pmol/mg protein) compared to ApoE−/− cells (36.19 ± 7.10, $p = 0.040$) (Fig 3C), indicating that MGL is the key enzyme in macrophage 2-AG homeostasis. Unchanged protein expression of CB2R (Fig. 3D), comparable cytosolic Ca^{2+} responses to 2-AG treatment and an only slightly lower relative response of DKO cells to the maximal, ATP-provoked Ca^{2+} flux (Fig. 3E–G) indicate that although DKO macrophages are unable to clear 2-AG as efficiently as ApoE−/

− cells, their EC system remains responsive to 2-AG rendering CB2R desensitization unlikely to occur. This finding contrasts CB1R desensitization in brain of MGL−/− mice [24,25].

3.4. Reduced foam cell formation in DKO macrophages

The formation of macrophage-derived foam cells is a hallmark in atherogenesis. Therefore, we determined lipid parameters and observed unaltered TG and CE (Fig. 4A) but reduced TC (ApoE: 41.5 ± 5.89 vs DKO: 31.4 ± 3.43 μg/mg protein, p = 0.0038, Fig. 4B) and FC (ApoE: 38.3 ± 6.77 vs DKO: 32.0 ± 2.77 μg/mg protein, p = 0.0465, Fig. 4C) concentrations under non-loaded conditions. Upon loading with very low-density lipoprotein (VLDL) and acetylated (ac)LDL, macrophages from DKO mice displayed significant reductions in TG (ApoE−/− + VLDL: 122 ± 9.36 vs DKO + VLDL: 93.7 ± 15.6 μg/mg protein, p = 0.005; ApoE−/− + acLDL: 25.3 ± 2.93 vs DKO + acLDL: 17.2 ± 5.09 μg/mg protein, p = 0.01; Fig. 4A) and cholesterol concentrations (Fig. 4B–D). Nile red staining of lipid droplets confirmed our observation of reduced foam cell formation upon lipoprotein loading of DKO macrophages (Fig. 4E). mRNA expression of Cd36 (involved in fatty acid and lipoprotein uptake) was reduced by 32% (p = 0.0005). mRNA levels of Msr1 (also known as scavenger receptor A), Sr-B1 (bidirectional cholesterol transporter), and the ABC transporters Abca1 and Abcg1 (responsible for cholesterol efflux from the cells) were unaltered (Fig. 4F). In accordance, cholesterol efflux toward HDL_3 and ApoA-I as acceptors was unchanged (Fig. 4G). Co-incubation of macrophages with acLDL and the CB2R inverse agonist SR144528 partially reverses the observed foam cell formation in DKO cells, suggesting that this effect is at least in part mediated by CB2R signaling (Fig. S2A, B). Comparable apoptosis and necrosis (Supplementary Fig. S2C–E), mRNA expression levels of M1/M2 polarization markers (Supplementary Fig. S2F), adhesion molecule ligands, matrix metalloproteinase inhibitors (Supplementary Fig. S2G), and *in vivo* phagocytic activity of fluorescently labeled *E. coli* particles (Supplementary Fig. S2H) argue against profound changes in macrophage phenotype and function caused by alterations in 2-AG concentrations in the circulation. Interestingly, when loaded with acLDL, DKO macrophages have reduced mRNA expression of pro-inflammatory IL-6 and increased expression of anti-inflammatory IL-10 (Fig. 4H) compared to ApoE−/− cells, indicating a polarization toward M2-like macrophages.

3.5. Alterations in the aortic EC signaling in DKO mice

In the aortae, 2-AG concentrations were 3.5-fold increased in DKO compared to ApoE−/− mice (p < 0.0001; Fig. 5A). Quantitative real-time PCR analyses revealed reduced expression of Cb1r by 49% (p = 0.015) and Cb2r by 56% (p = 0.0259) in abdominal aortae of DKO compared to ApoE−/− mice after 9 weeks of WTD feeding. Expression levels of adhesion molecules such as P-selectin, E-selectin, L-selectin, vascular cell adhesion molecule-1, and intra-cellular adhesion molecule-1 (Fig. 5B) as well as matrix metalloproteinase (Mmp)-2 and Mmp-9 were comparable between both genotypes. However, transcript levels of (Timp)-1 and Timp-2 were significantly increased by 5.1-fold (p = 0.022) and 1.3-fold (p = 0.011), respectively, in DKO aortae compared to ApoE−/− aortae (Fig. 5B), indicating increased inhibition of gelatinolytic enzymes in the aortic tissue of DKO mice. Of note, mRNA expression levels of Mcp-1 and IL-1β were increased,

whereas Mcp-5, Tnf-α, IL-6, and Cox-2 remained at comparable expression levels between DKO and ApoE−/− aortae (Fig. 5C).

3.6. Enhanced lesion size with increased plaque stability in DKO mice

Interestingly, we found increased plaque size in *en face* aortae of DKO compared to ApoE−/− mice (Fig. 5D) in total thoracic aorta (ApoE−/−: 9.44 ± 3.71 vs DKO: 12.7 ± 3.87%, p = 0.028, Fig. 5E) and arch area (ApoE−/−: 18.1 ± 7.56 vs DKO: 24.6 ± 6.70%, p = 0.022, Fig. 5F). The increase in plaque burden was even more pronounced in aortic valve sections of DKO mice (ApoE−/−: 0.232 ± 0.073 vs DKO: 0.345 ± 0.09 mm^2, p = 0.001, Fig. 6A). However, the relative abundance of neutral lipids within the lesions was reduced in DKO plaques, as visualized by diminished Oil red O staining (ApoE−/−: 75.4 ± 12.5 vs DKO: 66.7 ± 7.95%, p = 0.031, Fig. 6B). Since macrophage-derived foam cells are the major component of lesional lipid accumulation, we performed MoMa-2 immunostaining, which revealed a trend to 19% reduced amount of macrophages in DKO lesions (p = 0.061; Fig. 6C). This finding phenocopies our *in vitro* data with reduced foam cell formation in DKO macrophages (Fig. 4A,B), indicating that another plaque component strongly contributes to the increase in plaque size and relative plaque composition of DKO mice. Indeed, collagen content (measured by Masson's Trichrome staining) was 1.6-fold increased in DKO plaques (p = 0.0007), comprising almost 40% of the total lesion area (Fig. 6D). Concomitantly fibrous caps were 1.8-fold thicker (p = 0.0032) in DKO plaques (Fig. 6E) This elevated amount of collagen was likely caused by the increased abundance of smooth muscle cells within the plaque (ApoE−/−: 2.91 ± 1.15 vs DKO: 4.20 ± 1.49%, p = 0.0155; Fig. 6F and Supplementary Fig. S3). Gelatinolytic activities of conditioned media from cultivated peritoneal neutrophils, the most important cell type responsible for plaque destabilization, showed comparable activities of pro-MMP-9, MMP-9, pro-MMP-2, and MMP-2 (Supplementary Fig. S4). Relative abundance of active caspase-3 was comparable between both genotypes (p = 0.742) (Fig. 6G and Supplementary Fig. S5). Neovessel formation determined by anti-CD31 immunohistochemistry (Fig. 6H) was absent in the plaques of both genotypes. Interestingly, necrotic core size was reduced in DKO (13.7 ± 9.73%) compared to ApoE−/− mice (18.7 ± 6.41, p = 0.052) (Fig. 6H). Of note, the ratio of collagen to necrotic core, an important indicator of plaque stability [31], was 2.5-fold increased (p = 0.0003) (Fig. 6J), whereas the ratio of necrotic core to smooth muscle cells as an indicator of plaque vulnerability was reduced by 53% in DKO animals (p = 0.0025) (Fig. 6K). These results suggest that although DKO mice exhibit larger lesions, their atheroma composition (Fig. 6L) is favorably changed to a more stable plaque phenotype.

3.7. Plaque phenotype in DKO mice is reversed upon SR144528 treatment

To determine the role of CB2R activation in DKO mice *in vivo*, we treated ApoE−/− and DKO mice with the CB2R inverse agonist SR144528 during the last three weeks of 8 week WTD feeding. We found no difference in peripheral blood cell counts between DKO and ApoE−/− mice (Fig. 7A), indicating that CB2R activation mediates leukocytosis in DKO mice during WTD feeding. In addition, we found comparable plaque size between ApoE−/− and DKO mice upon chronic CB2R blockade (ApoE−/−: 0.285 ± 0.072 vs DKO: 0.300 ± 0.046 mm^2, p = 0.68, Fig. 7B). Moreover, all beneficial changes in plaque structure were completely absent in DKO compared to control mice upon SR144528 treatment, as

evidenced by comparable abundance of neutral lipids within plaque lesions (ApoE−/−: 57.8 ± 3.0 vs DKO: 61.8 ± 7.5%, p = 0.25, Fig. 7C), macrophages (ApoE−/− 32.4 ± 9.3 vs DKO: 35.7 ± 3.6%, p = 0.44, Fig. 7D), collagen (ApoE−/−: 25.4 ± 6.3 vs DKO: 24.4 ± 6.2%, p = 0.80, Fig. 7E), and necrotic core (ApoE−/−: 15.8 ± 5.4 vs DKO: 15.3 ± 7.6%, p = 0.92, Fig. 7F). These results unequivocally confirm that the observed phenotype in DKO mice originates from CB2R activation.

4. Discussion

MGL is the rate-limiting enzyme for the breakdown of MG and, specifically, of the EC 2-AG in multiple tissues including the brain. Thus, MGL plays a central role in lipid and energy metabolism as well as 2-AG turnover and signaling [26]. Due to multiple effects of EC signaling on energy homeostasis and immune response, we speculated that the lack of MGL may also affect the pathogenesis of atherosclerosis. To investigate the consequences of MGL deficiency on atherosclerosis development, we generated MGL−/− mice on the atherosclerotic ApoE−/− background and challenged them with WTD.

We found systemically increased 2-AG concentrations in the DKO mice, indicating that MGL is capable to efficiently regulate 2-AG homeostasis. However, expected cannabimimetic effects mediated by CB1R such as increased food intake and body adiposity were absent in DKO animals. These results phenocopy the state of MGL−/− mice, in which increased brain 2-AG levels do not promote CB1R-mediated signaling due to receptor desensitization via receptor downregulation and blunting of cannabimimetic signaling [24-26]. As expected in the CB1R-desensitized model, plasma lipid profiles remained unaltered between the genotypes, suggesting that lipid homeostasis is unaffected.

Little is known about the CB2R activity in states of chronic 2-AG elevation. Chanda et al. stated that CB2R densities remain unaltered in spleen of MGL−/− mice [24], but to date no functional assay addressed the influence of systemically increased 2-AG levels on CB2R-expressing cells. mRNA expression of other lipases capable to degrade MGs and enzymes responsible for 2-AG generation remained unchanged in the absence of MGL. Our results indicate that MGL represents the key enzyme responsible for MG hydrolysis and 2-AG deactivation in macrophages, since MG hydrolase activity was reduced by 44% and cellular 2-AG content was increased 75% in DKO macrophages compared to the control cells. To assess a possible CB2R desensitization, we performed a functional measurement of CB2R activation in macrophages by stimulating cells with 2-AG and measuring cytosolic Ca^{2+} levels. Unchanged cellular Ca^{2+} response to 2-AG treatment indicates that DKO macrophages retain their full functionality of CB2R and its signaling cascade with no evidence of receptor desensitization. Although DKO mice have systemically elevated 2-AG levels, CB2R-mediated signaling remains fully functional. Thus, increased 2-AG concentrations can potentiate cannabimimetic effects on CB2R-expressing immune cells. As previously proposed, CB1R may be more prone to the process of desensitization [32].

Elevated leukocyte numbers in the DKO mice indicate that MGL deficiency affects immune functions and hematopoiesis *in vivo*, which may be a result of altered EC signaling. The increase in leukocyte numbers may originate from extended WBC half-life and the

potentiated hematopoiesis of LSK cells in the bone marrow of DKO mice. Indeed, CB2R activation in the bone marrow was shown to stimulate stress-induced hematopoiesis by increasing the marrow cellularity, LSK numbers, and bone marrow cell survival [33]. Importantly, when we chronically treated mice with SR144528 to block CB2R activation, we failed to observe any differences in circulating WBC counts between ApoE−/− and DKO mice, demonstrating that CB2R signaling is responsible for the observed effect.

Detectable plasma 2-AG levels and significantly elevated 2-AG concentrations in the aorta of DKO mice, together with decreased Cb1r and Cb2r mRNA expression in aortae of DKO mice, suggest systemic and local changes in EC signaling. Interestingly, we observed elevated mRNA expression of Mcp-1 and IL-1β in aortae of DKO mice. This finding may be attributed to the reduced Cb2r mRNA expression in the vascular tissue, leading to an elevated inflammatory propensity due to reduction of anti-inflammatory effects of CB2R activation in the aorta.

En face and aortic valve section analyses demonstrated increased plaque formation with reduced lipid content in DKO compared to ApoE−/− mice. Macrophage-derived foam cell formation is considered to be a hallmark of atherosclerosis due to subintimal macrophage accumulation and removal of modified lipoprotein particles in an uncontrolled manner. Intraplaque macrophage amount and intracellular TG and cholesterol concentrations were reduced in DKO mice. Reduced Cd36 mRNA expression and unchanged cholesterol efflux in DKO macrophages indicate that decreased lipoprotein uptake rather than increased lipid efflux is likely responsible for reduced foam cell formation of DKO macrophages. In line with our data, CB2R activation in human macrophages leads to downregulation of CD36, causing reduced foam cell formation [34]. This effect is only in part attributable to CB2R activation, since co-treatment with SR144528 normalizes TC but not TG concentrations in DKO macrophages. Changes in intracellular lipid homeostasis also modulate functions of macrophages as important members of the innate immunity. Macrophage FC accumulation triggers macrophage apoptosis [35], which in turn affects atherosclerosis progression, leading to necrotic core formation and reduction in efficient removal of cellular debris [36]. Apoptosis, however, seems to be unaltered between ApoE−/− and DKO mice. (i) In thioglycolate-elicited DKO and ApoE−/− macrophages, we observed comparable annexin V/PI staining after *in vitro* loading with VLDL or acLDL, indicating comparable levels of apoptosis and necrosis. (ii) Caspase-3 immunohistochemistry of aortic valve sections revealed unaltered apoptosis *in vivo*. (iii) Caspase-3 western blotting of aortae confirmed the results. Beside reduced foam cell formation, macrophage phenotype and functions of DKO macrophages are unaltered, as evidenced by comparable M1/M2 polarization, integrin expression, and phagocytic activity to ApoE−/− cells. DKO macrophages exposed to acLDL, however, have reduced mRNA expression of IL-6 and increased expression of IL-10, indicating an M2-like phenotype.

An important process in plaque pathogenesis is the formation of a fibrous cap, which protects the necrotic core from rupture and stabilizes the lesion. Vulnerable plaques are characterized by decreasing amounts of fibrous cap collagen, increase in foam cell formation, and build-up of the necrotic core (reviewed in [37,38]). A thinning fibrous cap decreases lesion stability, rendering atherosclerotic plaques susceptible to rupture and

thrombus formation [39]. Thus, reducing the ratio of collagen to necrotic core is an indicator of decreased plaque stability [31]. Destabilization of plaques due to neovessel formation was absent in both ApoE−/− and DKO mice. Of note, the necrotic core area, which contributes to inflammation, proteolytic plaque breakdown, and physical stress on the fibrous cap [39], was reduced in plaques of DKO mice. Major determinants for the amount of plaque collagen content and thus plaque stability are collagen production (caused by infiltrating smooth muscle cells) and degradation (mediated by neutrophil-produced matrix metalloproteinases). Importantly, we found markedly increased collagen content in lesions of DKO mice, with a relative collagen amount comprising almost 40% of the atherosclerotic plaque. Comparable mRNA expression levels of Mmp-2 and -9 together with unchanged gelatinolytic capacities of (pro-) MMP-2 and -9 from DKO neutrophil conditioned media argue against changes in production of MMPs. Increased mRNA expression of aortic Timp-1 and Timp-2 may be a contributing factor for hindered matrix degradation. However, the increase in collagen plaque content of DKO mice is most likely attributable to the increased abundance of smooth muscle cells, indicating either increased migration of smooth muscle cells from the media into subintimal areas or prolonged survival within the lesions. Importantly, all changes in DKO plaque phenotype were completely reversed by chronic CB2R antagonism with SR144528, indicating that the observed effects are due to potentiated EC signaling on CB2R expressing cells. Although CB2R antagonism reduced DKO plaque size to the levels found in ApoE−/− mice, the lesions were rendered more unstable with as little as 24% of total lesion size being attributed to collagen.

It has previously been shown that chronic administration of low doses of THC reduces plaque size [15]. However, little is known about plaque stability and collagen content in this setting. We argue to consider these data with caution since (i) THC is only a partial agonist on CB2R even capable to antagonize the receptor activation by agonists [40], (ii) administration of the drug can lead to a range of cannabimimetic effects on CB1R prior the development of tolerance, and (iii) THC is capable of mediating the effects distinct of the ones mediated by endogenous CB2R ligands (reviewed in [41,42]). Interestingly, recent work by Steffens and colleagues reported an opposite plaque phenotype to our DKO mice in ApoE−/−FAAH−/− mice [43]. FAAH efficiently degrades anandamide, the second molecule identified as potential EC. The authors found reduced plaque size with comparable amount of macrophages and decreased plaque stability in ApoE−/−FAAH−/− compared to ApoE−/− mice. Surprisingly, elevation in plasma anandamide concentrations in ApoE−/−FAAH−/− mice was accompanied by a reduction in 2-AG concentrations [43]. It is therefore tempting to speculate that the plaque phenotype in ApoE−/−FAAH−/− mice may be an indirect consequence of decreased 2-AG levels and blunted 2-AG-mediated CB2R signaling instead of increased anandamide concentrations *per se*, since (i) tissue 2-AG levels are by far more abundant than anandamide with nanomolar *versus* picomolar concentrations (reviewed in [41]), (ii) 2-AG is a full whereas anandamide is a partial CBR agonist, which is also capable to attenuate the effectiveness of 2-AG to activate CB2R [6], and (iii) structure–activity relationship studies suggested that 2-AG rather than anandamide is the true natural ligand for both CB1R and CB2R [44,45]. Thus, it may be plausible that MGL and 2-AG are the key regulators of EC homeostasis in atherosclerosis, whereas FAAH and anandamide may act indirectly, mediating its effects on atherogenesis via modulations in 2-AG signaling.

Europe PMC Funders Author Manuscripts

In summary, our data provide evidence that genetic ablation of MGL causes alterations in EC signaling, thereby indirectly affecting atherogenesis. Despite elevated 2-AG concentrations, CB2R-mediated signaling remains fully functional, arguing against CB2R desensitization. We conclude that lack of MGL modulates EC signaling in CB2R-expressing cells and influences (patho)physiological processes, which concomitantly affect the pathogenesis of atherosclerosis. Selective CB2R activation within atherosclerotic plaques has already been suggested to represent a promising strategy for reducing atherosclerotic inflammation and related plaque vulnerability [46]. Chronic MGL inhibition may be a novel therapeutic intervention in atherosclerosis treatment, leading to formation of less vulnerable atherosclerotic plaques.

Supplementary Material

Refer to Web version on PubMed Central for supplementary material.

Acknowledgments

This work was supported by grants from the Austrian Science Fund (FWF) (DK-MCD W1226, SFB-LIPOTOX F3004, P22832, P27070, P25193) and the PhD program “Molecular Medicine” of the Medical University of Graz. The authors thank A. Ibovnik, and M. Absenger-Novak for excellent technical assistance and I. Hindler for mice care.

Abbreviations

2-AG	2-arachidonoyl glycerol
ApoE	apolipoprotein E
CBR	cannabinoid receptor
DKO	double-knockout
EC	endocannabinoid
MG	monoglyceride
MGL	monoglyceride lipase
THC	Δ^9-tetrahydrocannabinol
TG	triglyceride
WBC	white blood cell
WTD	Western-type diet

References

[1]. Zechner R, Zimmermann R, Eichmann TO, Kohlwein SD, Haemmerle G, Lass A, Madeo F. FAT SIGNALS–lipases and lipolysis in lipid metabolism and signaling. Cell Metab. 2012; 15:279–291. [PubMed: 22405066]

[2]. Strand O, Vaughan M, Steinberg D. Rat adipose tissue lipases: hormone-sensitive lipase activity against triglycerides compared with activity against lower glycerides. J. Lipid Res. 1964; 5:554–562. [PubMed: 14221100]

[3]. Goparaju SK, Ueda N, Yamaguchi H, Yamamoto S. Anandamide amidohydrolase reacting with 2-arachidonoylglycerol, another cannabinoid receptor ligand. FEBS Lett. 1998; 422:69–73. [PubMed: 9475172]

[4]. Blankman JL, Simon GM, Cravatt BF. A comprehensive profile of brain enzymes that hydrolyze the endocannabinoid 2-arachidonoylglycerol. Chem. Biol. 2007; 14:1347–1356. [PubMed: 18096503]

[5]. Savinainen JR, Jarvinen T, Laine K, Laitinen JT. Despite substantial degradation, 2-arachidonoylglycerol is a potent full efficacy agonist mediating CB(1) receptor-dependent G-protein activation in rat cerebellar membranes. Br. J. Pharmacol. 2001; 134:664–672. [PubMed: 11588122]

[6]. Gonsiorek W, Lunn C, Fan X, Narula S, Lundell D, Hipkin RW. Endocannabinoid 2-arachidonyl glycerol is a full agonist through human type 2 cannabinoid receptor: antagonism by anandamide. Mol. Pharmacol. 2000; 57:1045–1050. [PubMed: 10779390]

[7]. Williams CM, Kirkham TC. Reversal of delta 9-THC hyperphagia by SR141716 and naloxone but not dexfenfluramine. Pharmacol. Biochem. Behav. 2002; 71:333–340. [PubMed: 11812541]

[8]. Osei-Hyiaman D, DePetrillo M, Pacher P, Liu J, Radaeva S, Batkai S, Harvey-White J, Mackie K, Offertaler L, Wang L, Kunos G. Endocannabinoid activation at hepatic CB1 receptors stimulates fatty acid synthesis and contributes to diet-induced obesity. J. Clin. Invest. 2005; 115:1298–1305. [PubMed: 15864349]

[9]. Osei-Hyiaman D, Liu J, Zhou L, Godlewski G, Harvey-White J, Jeong WI, Batkai S, Marsicano G, Lutz B, Buettner C, Kunos G. Hepatic CB1 receptor is required for development of diet-induced steatosis, dyslipidemia, and insulin and leptin resistance in mice. J. Clin. Invest. 2008; 118:3160–3169. [PubMed: 18677409]

[10]. Tiyerili V, Zimmer S, Jung S, Wassmann K, Naehle CP, Lutjohann D, Zimmer A, Nickenig G, Wassmann S. CB1 receptor inhibition leads to decreased vascular AT1 receptor expression, inhibition of oxidative stress and improved endothelial function. Basic Res. Cardiol. 2010; 105:465–477. [PubMed: 20361197]

[11]. Dol-Gleizes F, Paumelle R, Visentin V, Mares AM, Desitter P, Hennuyer N, Gilde A, Staels B, Schaeffer P, Bono F. Rimonabant, a selective cannabinoid CB1 receptor antagonist, inhibits atherosclerosis in LDL receptor-deficient mice. Arterioscler. Thromb. Vasc. Biol. 2009; 29:12–18. [PubMed: 18845788]

[12]. Lu T, Newton C, Perkins I, Friedman H, Klein TW. Cannabinoid treatment suppresses the T-helper cell-polarizing function of mouse dendritic cells stimulated with Legionella pneumophila infection. J. Pharmacol. Exp. Ther. 2006; 319:269–276. [PubMed: 16837556]

[13]. Buckley NE, McCoy KL, Mezey E, Bonner T, Zimmer A, Felder CC, Glass M. Immunomodulation by cannabinoids is absent in mice deficient for the cannabinoid CB(2) receptor. Eur. J. Pharmacol. 2000; 396:141–149. [PubMed: 10822068]

[14]. Sacerdote P, Massi P, Panerai AE, Parolaro D. In vivo and in vitro treatment with the synthetic cannabinoid CP55, 940 decreases the in vitro migration of macrophages in the rat: involvement of both CB1 and CB2 receptors. J. Neuroimmunol. 2000; 109:155–163. [PubMed: 10996217]

[15]. Steffens S, Veillard NR, Arnaud C, Pelli G, Burger F, Staub C, Karsak M, Zimmer A, Frossard JL, Mach F. Low dose oral cannabinoid therapy reduces progression of atherosclerosis in mice. Nature. 2005; 434:782–786. [PubMed: 15815632]

[16]. Klein TW, Newton C, Friedman H. Cannabinoid receptors and immunity. Immunol. Today. 1998; 19:373–381. [PubMed: 9709506]

[17]. McKallip RJ, Lombard C, Martin BR, Nagarkatti M, Nagarkatti PS. Delta(9)-tetrahydrocannabinol-induced apoptosis in the thymus and spleen as a mechanism of immunosuppression in vitro and in vivo. J. Pharmacol. Exp. Ther. 2002; 302:451–465. [PubMed: 12130702]

[18]. Zhu W, Friedman H, Klein TW. Delta9-tetrahydrocannabinol induces apoptosis in macrophages and lymphocytes: involvement of Bcl-2 and caspase-1. J. Pharmacol. Exp. Ther. 1998; 286:1103–1109. [PubMed: 9694974]

[19]. Delsing DJ, Leijten FP, Arts K, van Eenennaam H, Garritsen A, Gijbels MJ, de Winther MP, van Elsas A. Cannabinoid receptor 2 deficiency in haematopoietic cells aggravates early

Europe PMC Funders Author Manuscripts

atherosclerosis in LDL receptor deficient mice. Open Cardiovasc. Med. J. 2011; 5:15–21. [PubMed: 21660251]

[20]. Hoyer FF, Steinmetz M, Zimmer S, Becker A, Lutjohann D, Buchalla R, Zimmer A, Nickenig G. Atheroprotection via cannabinoid receptor-2 is mediated by circulating and vascular cells in vivo. J. Mol. Cell Cardiol. 2011; 51:1007–1014. [PubMed: 21884703]

[21]. Zhao Y, Liu Y, Zhang W, Xue J, Wu YZ, Xu W, Liang X, Chen T, Kishimoto C, Yuan Z. WIN55212-2 ameliorates atherosclerosis associated with suppression of pro-inflammatory responses in ApoE-knockout mice. Eur. J. Pharmacol. 2010; 649:285–292. [PubMed: 20868672]

[22]. Montecucco F, Matias I, Lenglet S, Petrosino S, Burger F, Pelli G, Braunersreuther V, Mach F, Steffens S, Di Marzo V. Regulation and possible role of endocannabinoids and related mediators in hypercholesterolemic mice with atherosclerosis. Atherosclerosis. 2009; 205:433–441. [PubMed: 19187936]

[23]. Vaughan M, Berger JE, Steinberg D. Hormone-sensitive lipase and monoglyceride lipase activities in adipose tissue. J. Biol. Chem. 1964; 239:401–409. [PubMed: 14169138]

[24]. Chanda PK, Gao Y, Mark L, Btesh J, Strassle BW, Lu P, Piesla MJ, Zhang MY, Bingham B, Uveges A, Kowal D, Garbe D, Kouranova EV, Ring RH, Bates B, Pangalos MN, Kennedy JD, Whiteside GT, Samad TA. Monoacylglycerol lipase activity is a critical modulator of the tone and integrity of the endocannabinoid system. Mol. Pharmacol. 2010; 78:996–1003. [PubMed: 20855465]

[25]. Schlosburg JE, Blankman JL, Long JZ, Nomura DK, Pan B, Kinsey SG, Nguyen PT, Ramesh D, Booker L, Burston JJ, Thomas EA, Selley DE, Sim-Selley LJ, Liu QS, Lichtman AH, Cravatt BF. Chronic monoacylglycerol lipase blockade causes functional antagonism of the endocannabinoid system. Nat. Neurosci. 2010; 13:1113–1119. [PubMed: 20729846]

[26]. Taschler U, Radner FP, Heier C, Schreiber R, Schweiger M, Schoiswohl G, Preiss-Landl K, Jaeger D, Reiter B, Koefeler HC, Wojciechowski J, Theussl C, Penninger JM, Lass A, Haemmerle G, Zechner R, Zimmermann R. Monoglyceride lipase deficiency in mice impairs lipolysis and attenuates diet-induced insulin resistance. J. Biol. Chem. 2011; 286:17467–17477. [PubMed: 21454566]

[27]. Knittelfelder OL, Weberhofer BP, Eichmann TO, Kohlwein SD, Rechberger GN. A versatile ultra-high performance LC-MS method for lipid profiling. J. Chromatogr. B Anal. Technol. Biomed. Life Sci. 2014; 951–952:119–128. [PubMed: 24548922]

[28]. Waldeck-Weiermair M, Jean-Quartier C, Rost R, Khan MJ, Vishnu N, Bondarenko AI, Imamura H, Malli R, Graier WF. Leucine zipper EF hand-containing transmembrane protein 1 (Letm1) and uncoupling proteins 2 and 3 (UCP2/3) contribute to two distinct mitochondrial Ca^{2+} uptake pathways. J. Biol. Chem. 2011; 286:28444–28455. [PubMed: 21613221]

[29]. Goeritzer M, Schlager S, Radovic B, Madreiter CT, Rainer S, Thomas G, Lord CC, Sacks J, Brown AL, Vujic N, Obrowsky S, Sachdev V, Kolb D, Chandak PG, Graier WF, Sattler W, Brown JM, Kratky D. Deletion of CGI-58 or adipose triglyceride lipase differently affects macrophage function and atherosclerosis. J. Lipid Res. 2014; 55:2562–2575. [PubMed: 25316883]

[30]. Kratzer A, Buchebner M, Pfeifer T, Becker TM, Uray G, Miyazaki M, Miyazaki-Anzai S, Ebner B, Chandak PG, Kadam RS, Calayir E, Rathke N, Ahammer H, Radovic B, Trauner M, Hoefler G, Kompella UB, Fauler G, Levi M, Levak-Frank S, Kostner GM, Kratky D. Synthetic LXR agonist attenuates plaque formation in apoE−/− mice without inducing liver steatosis and hypertriglyceridemia. J. Lipid Res. 2009; 50:312–326. [PubMed: 18812595]

[31]. Zhao Y, Ye D, Wang J, Calpe-Berdiel L, Azzis SB, Van Berkel TJ, Van Eck M. Stage-specific remodeling of atherosclerotic lesions upon cholesterol lowering in LDL receptor knockout mice. Am. J. Pathol. 2011; 179:1522–1532. [PubMed: 21741939]

[32]. Lichtman AH, Blankman JL, Cravatt BF. Endocannabinoid overload. Mol. Pharmacol. 2010; 78:993–995. [PubMed: 20952498]

[33]. Jiang S, Fu Y, Avraham HK. Regulation of hematopoietic stem cell trafficking and mobilization by the endocannabinoid system. Transfusion. 2011; 51(Suppl. 4):65S–71S. [PubMed: 22074629]

[34]. Chiurchiu V, Lanuti M, Catanzaro G, Fezza F, Rapino C, Maccarrone M. Detailed characterization of the endocannabinoid system in human macrophages and foam cells, and anti-

inflammatory role of type-2 cannabinoid receptor. Atherosclerosis. 2014; 233:55–63. [PubMed: 24529123]

[35]. Yao PM, Tabas I. Free cholesterol loading of macrophages induces apoptosis involving the fas pathway. J. Biol. Chem. 2000; 275:23807–23813. [PubMed: 10791964]

[36]. Thorp E, Tabas I. Mechanisms and consequences of efferocytosis in advanced atherosclerosis. J. Leukoc. Biol. 2009; 86:1089–1095. [PubMed: 19414539]

[37]. Finn AV, Nakano M, Narula J, Kolodgie FD, Virmani R. Concept of vulnerable/unstable plaque. Arterioscler. Thromb. Vasc. Biol. 2010; 30:1282–1292. [PubMed: 20554950]

[38]. Santos-Gallego CG, Picatoste B, Badimon JJ. Pathophysiology of acute coronary syndrome. Curr. Atheroscler. Rep. 2014; 16:401. [PubMed: 24504549]

[39]. Moore KJ, Tabas I. Macrophages in the pathogenesis of atherosclerosis. Cell. 2011; 145:341–355. [PubMed: 21529710]

[40]. Bayewitch M, Rhee MH, Avidor-Reiss T, Breuer A, Mechoulam R, Vogel Z. (−)-Delta9-tetrahydrocannabinol antagonizes the peripheral cannabinoid receptor-mediated inhibition of adenylyl cyclase. J. Biol. Chem. 1996; 271:9902–9905. [PubMed: 8626625]

[41]. Sugiura T, Kishimoto S, Oka S, Gokoh M. Biochemistry, pharmacology and physiology of 2-arachidonoylglycerol, an endogenous cannabinoid receptor ligand. Prog. Lipid Res. 2006; 45:405–446. [PubMed: 16678907]

[42]. Miller AM, Stella N. CB2 receptor-mediated migration of immune cells: it can go either way. Br. J. Pharmacol. 2008; 153:299–308. [PubMed: 17982478]

[43]. Lenglet S, Thomas A, Soehnlein O, Montecucco F, Burger F, Pelli G, Galan K, Cravatt B, Staub C, Steffens S. Fatty acid amide hydrolase deficiency enhances intraplaque neutrophil recruitment in atherosclerotic mice. Arterioscler. Thromb. Vasc. Biol. 2013; 33:215–223. [PubMed: 23241405]

[44]. Sugiura T, Kodaka T, Nakane S, Miyashita T, Kondo S, Suhara Y, Takayama H, Waku K, Seki C, Baba N, Ishima Y. Evidence that the cannabinoid CB1 receptor is a 2-arachidonoylglycerol receptor. Structure-activity relationship of 2-arachidonoylglycerol, ether-linked analogues, and related compounds. J. Biol. Chem. 1999; 274:2794–2801. [PubMed: 9915812]

[45]. Sugiura T, Kondo S, Kishimoto S, Miyashita T, Nakane S, Kodaka T, Suhara Y, Takayama H, Waku K. Evidence that 2-arachidonoylglycerol but not N-palmitoylethanolamine or anandamide is the physiological ligand for the cannabinoid CB2 receptor. Comparison of the agonistic activities of various cannabinoid receptor ligands in HL-60 cells. J. Biol. Chem. 2000; 275:605–612. [PubMed: 10617657]

[46]. Montecucco F, Di Marzo V. At the heart of the matter: the endocannabinoid system in cardiovascular function and dysfunction. Trends Pharmacol. Sci. 2012; 33:331–340. [PubMed: 22503477]

Europe PMC Funders Author Manuscripts

Europe PMC Funders Author Manuscripts

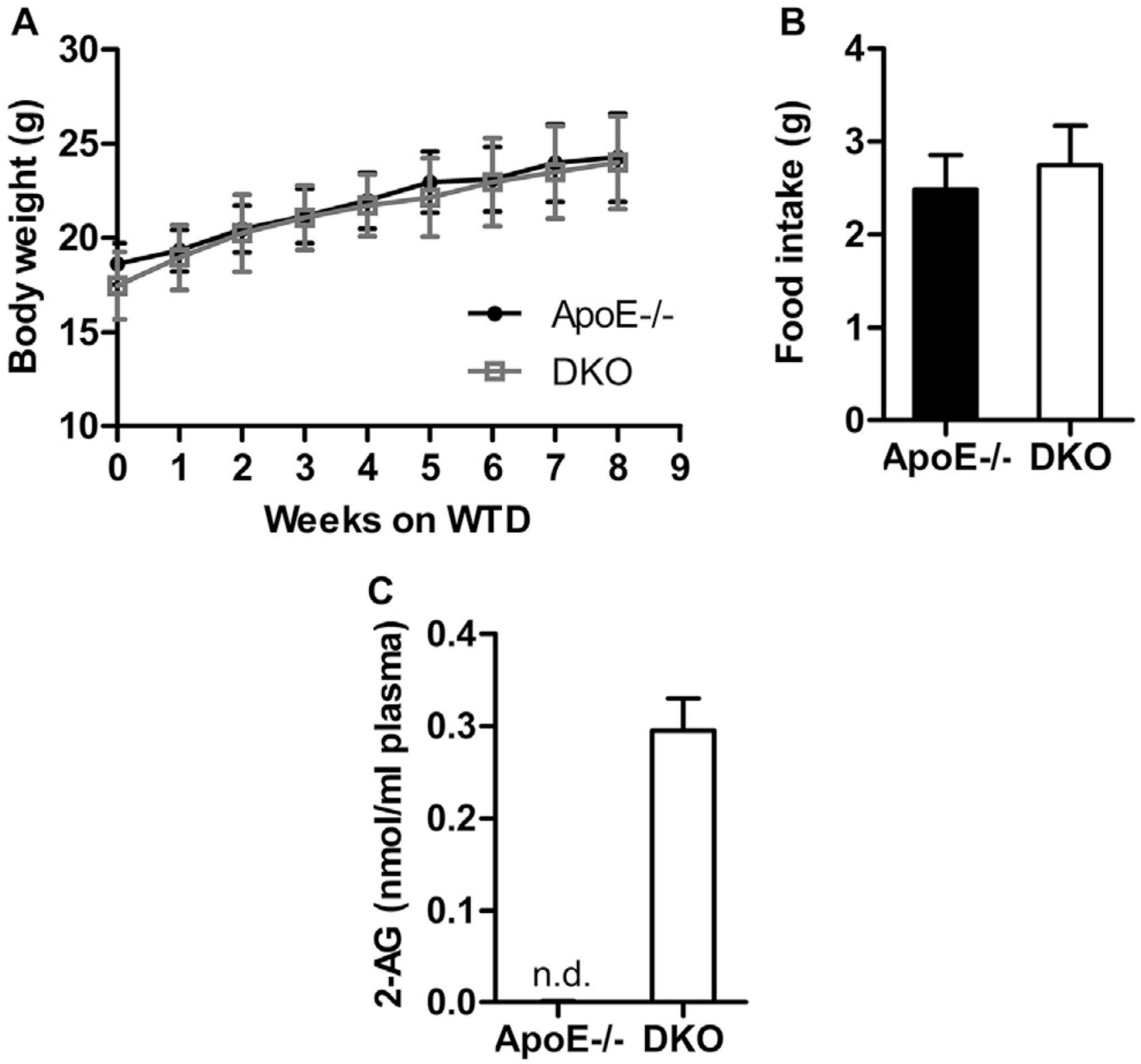

Fig. 1.

Increased plasma 2-AG concentrations in DKO mice. (A) Body weight (n = 14–15) and (B) food consumption of ApoE−/− and DKO mice (n = 5–7) during WTD feeding. Data represent means ± SD. (C) Plasma 2-AG concentrations after 9 weeks of WTD feeding. Data represent means (n = 5) + SD. n.d. not detectable.

Europe PMC Funders Author Manuscripts

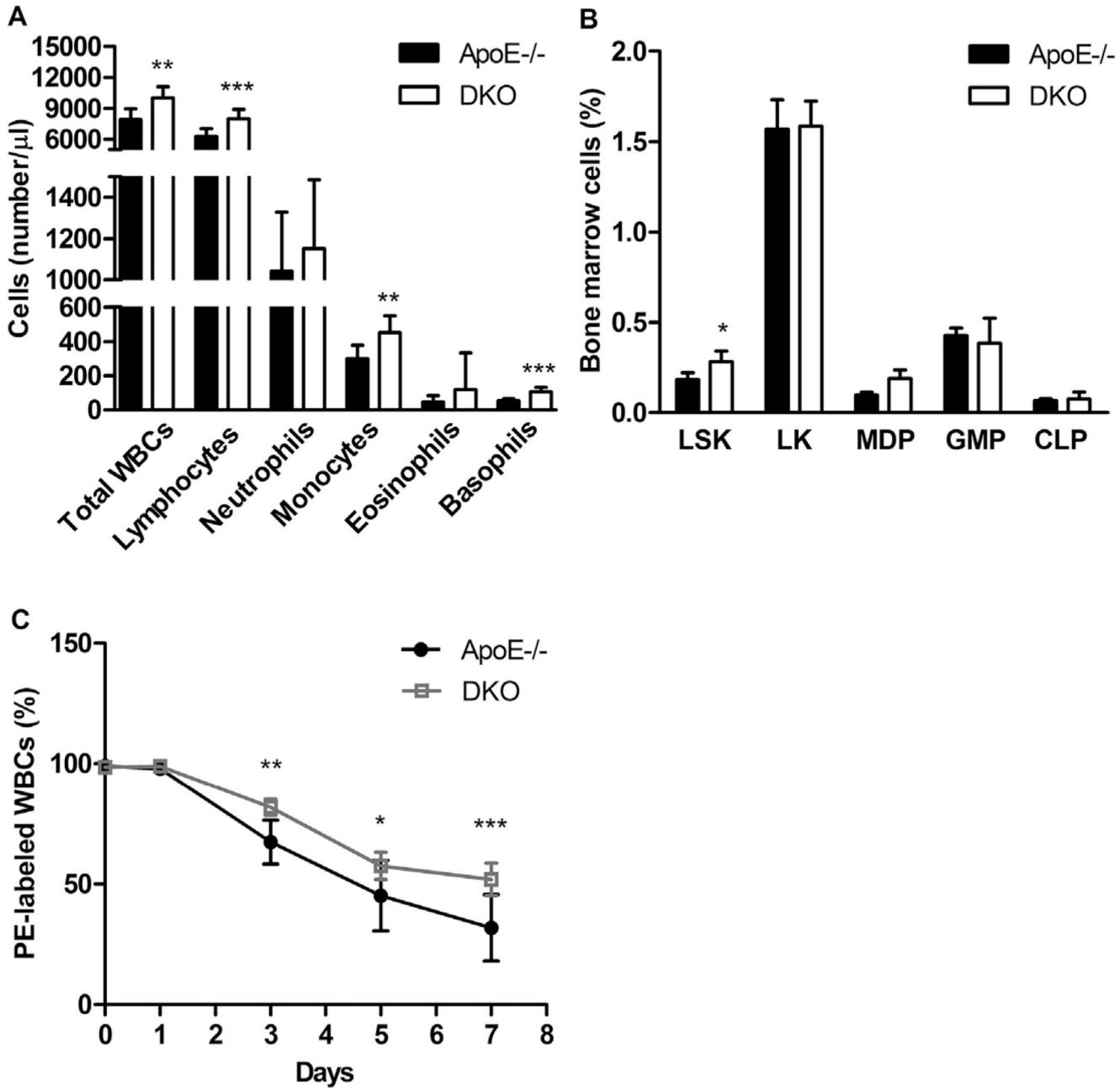

Fig. 2.

Increased circulating white blood cell (WBC) counts are associated with enhanced production and survival in DKO mice. (A) Absolute WBCs as means (n = 8–9) + SD. (B) Bone marrow analysis by flow cytometry: LSK populations ($Lin^{-}Sca\text{-}1^{+}c\text{-}Kit^{+}$), myeloid progenitor LK cells ($Lin^{-}Sca\text{-}1^{-}c\text{-}Kit^{+}$), granulocyte/monocyte progenitors (GMP; $Lin^{-}c\text{-}Kit^{+}CD34^{+}Fc\gamma RII/III^{+}$), monocyte/dendritic cell progenitors (MDP; $Lin^{-}c\text{-}Kit^{+/Int}CD115^{+}Flt3^{+}$), common lymphoid progenitors (CLP; $Lin^{-}c\text{-}Kit^{lo}Sca\text{-}1^{lo}IL7R\alpha^{+}$). Data represent means (n = 6–7) + SD. (C) Half life of WBCs as means (n = 7) ± SD. *, $p < 0.05$; **, $p \leq 0.01$; ***, $p \leq 0.001$.

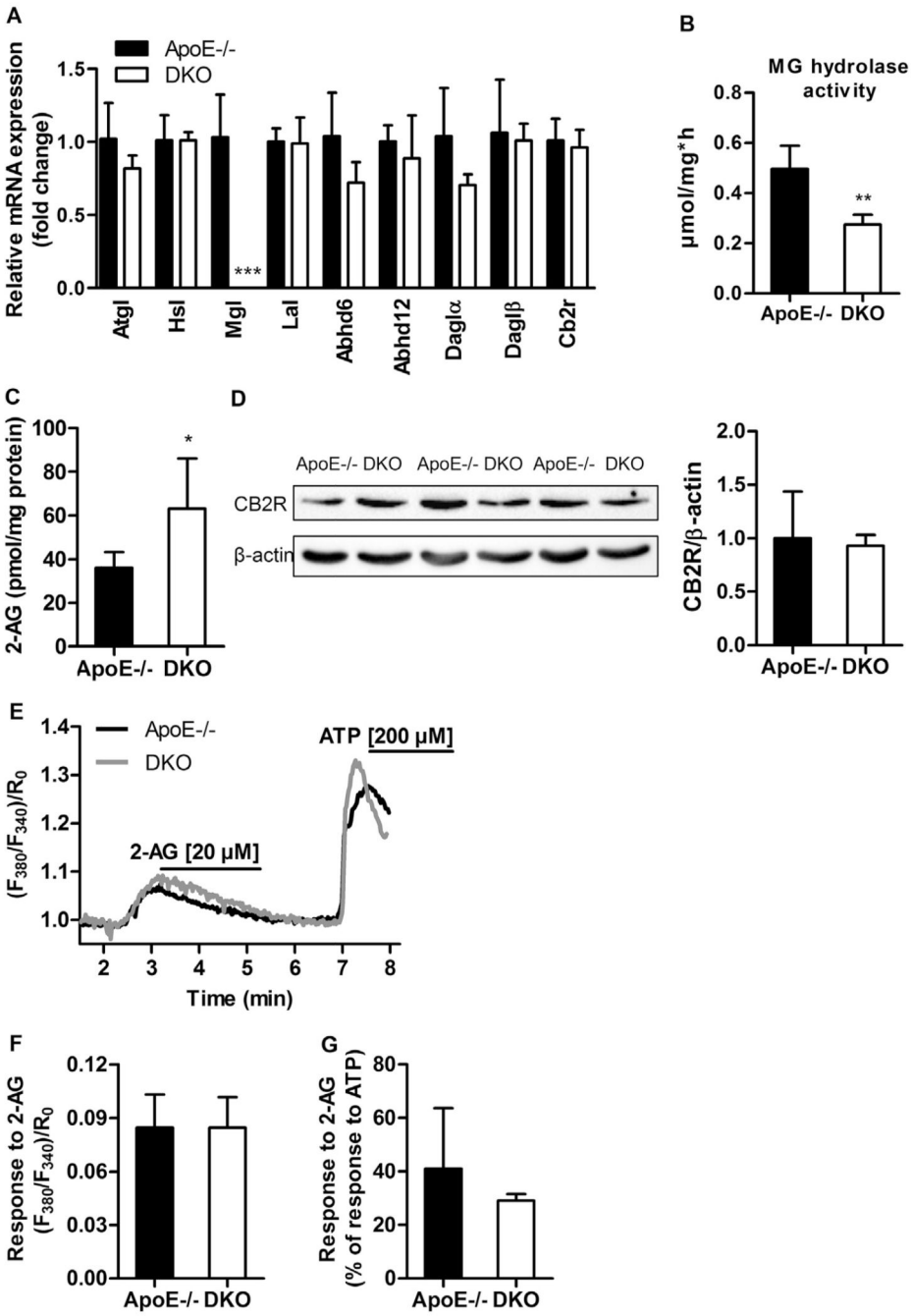

Fig. 3.

EC signaling is intact in DKO macrophages. (A) Macrophage mRNA expression was analyzed in duplicate by real-time PCR and normalized to Hprt expression as reference gene. Data represent means (n = 4–5) + SD. (B) MG hydrolase activity presented as means (n = 6) + SD. (C) Macrophage 2-AG concentrations presented as means (n = 6) + SD. (D) Western blot analysis of CB2R protein expression in macrophages. Densitometric quantification of CB2R/β-actin (loading control) represent means (n = 3) + SD. (E) Representative traces of cytosolic Ca^{2+} signals in macrophages upon stimulation with 20 μM

2-AG and 200 μM ATP shown as normalized ratio $(F_{380}/F_{340})/R_0$. (F) Statistical evaluation of Ca^{2+} signals in macrophages in response to 2-AG; (n = 4–6) + SD. (G) Cytosolic Ca^{2+} response of macrophages to 2-AG calculated as percentage of response to ATP; (n = 4–6) + SD. *, $p < 0.05$; **, $p \leq 0.01$; ***, $p \leq 0.001$.

Europe PMC Funders Author Manuscripts

Europe PMC Funders Author Manuscripts

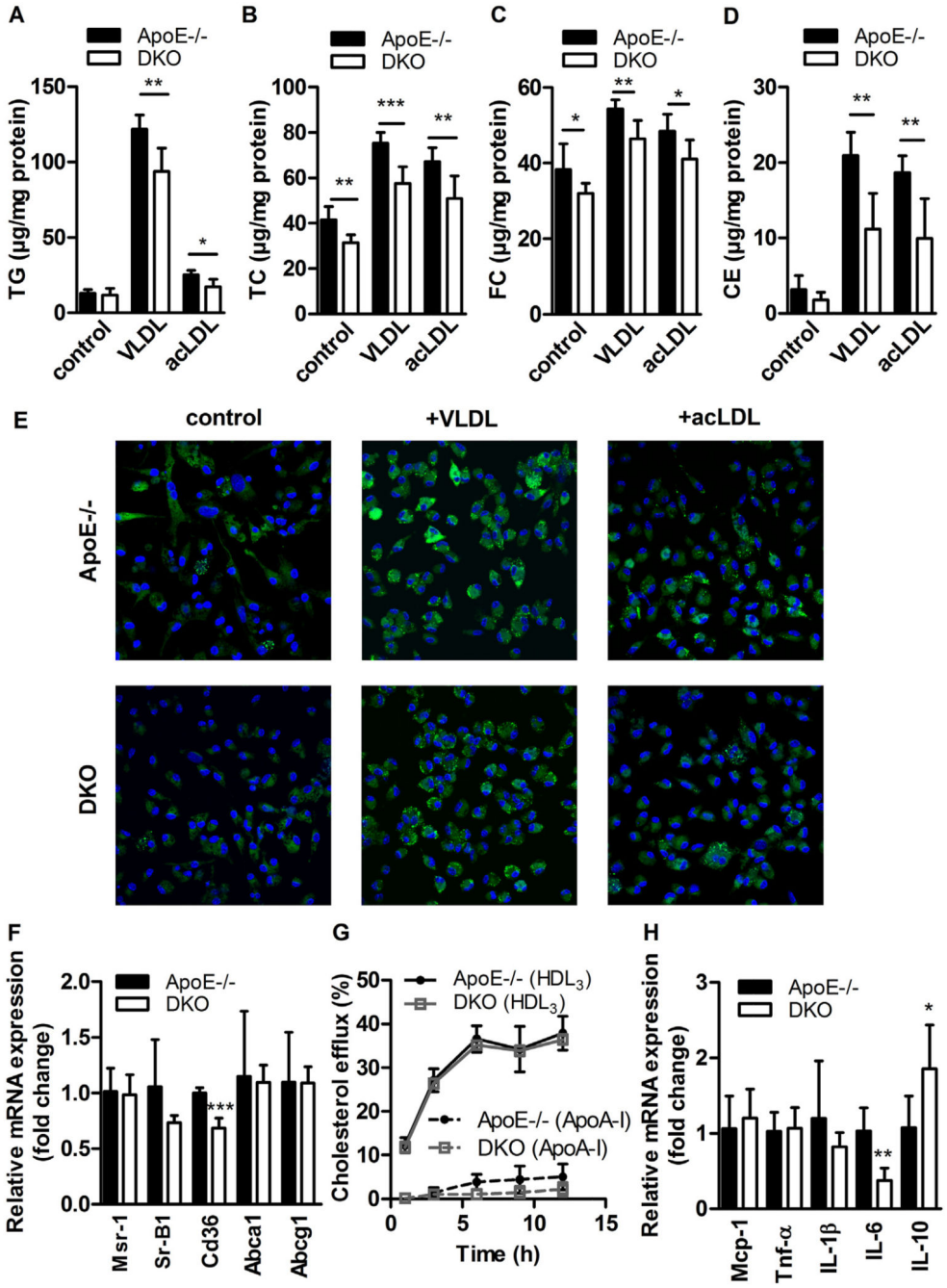

Fig. 4.

Reduced foam cell formation in DKO macrophages. Peritoneal macrophages were plated in 6-well plates for 24 h ± VLDL or acetylated (ac)LDL (100 µg protein/ml medium). After lipid extraction, (A) TG, (B) TC, and (C) FC concentrations were measured spectrophotometrically, and (D) CE concentrations were calculated as TC minus FC. Data represent means (n = 5–7) + SD. (E) Lipid droplets were visualized after Nile red staining (2.5 µg/ml) by confocal laser scanning microscopy. (F) mRNA expression of lipid transport genes analyzed in duplicate by real-time PCR and normalized to Hprt expression as

reference gene. Data represent means (n = 4–5) + SD. Relative mRNA expression and associated statistical parameters were determined by the $2^{-\Delta\Delta CT}$ method. (G) Cholesterol efflux to Apo-AI and HDL_3 expressed as the percentage of [^{3}H]cholesterol transferred from cells to the medium. Data show means (n = 3) ± SD of triplicate repeats. (H) mRNA expression of cytokines in macrophages treated with acLDL (100 μg protein/ml medium) for 24 h analyzed in duplicate by real-time PCR and normalized to Hprt expression as reference gene. Data represent means (n = 3–5) + SD. *, $p < 0.05$; **, $p \leq 0.01$; ***, $p \leq 0.001$.

Europe PMC Funders Author Manuscripts

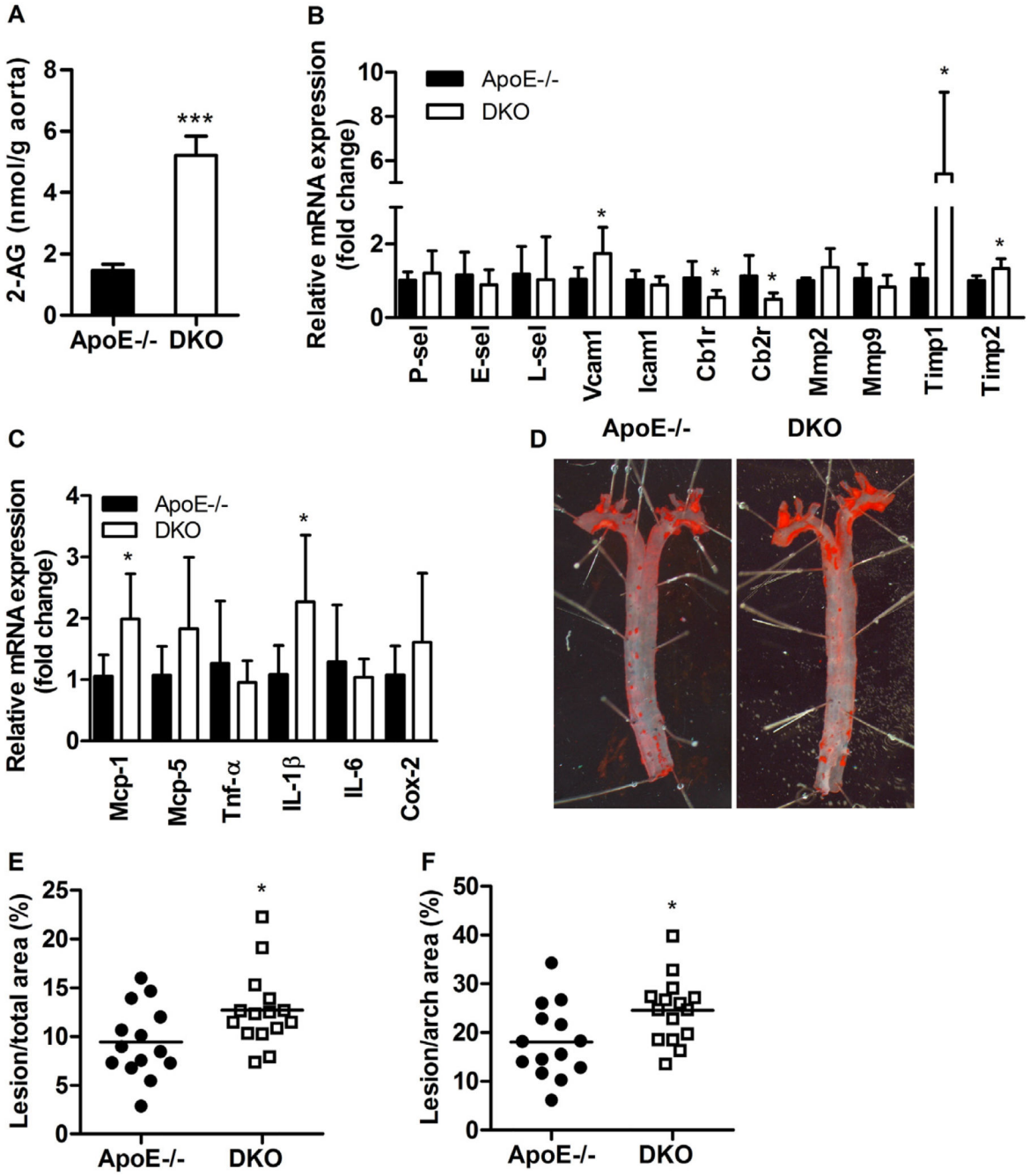

Fig. 5.

Increased 2-AG concentrations and plaque size in aortae of DKO mice. (A) Aortic 2-AG concentrations after 9 weeks of WTD feeding presented as means (n = 5) + SD. (B, C) mRNA expression analyzed in duplicate by real-time PCR and normalized to cyclophilin A expression as reference gene. Expression profiles and associated statistical parameters were determined by the $2^{-\Delta\Delta CT}$ method. Data represent means (n = 6–8) + SD. (D) Oil red O (ORO) staining of *en face* aortae. Quantification of lesion sizes in (E) total thoracic aortae

and (F) arch area. Bars represent means of 14–15 mice per group. *, $p < 0.05$; ***, $p \leq 0.001$.

Europe PMC Funders Author Manuscripts

Europe PMC Funders Author Manuscripts

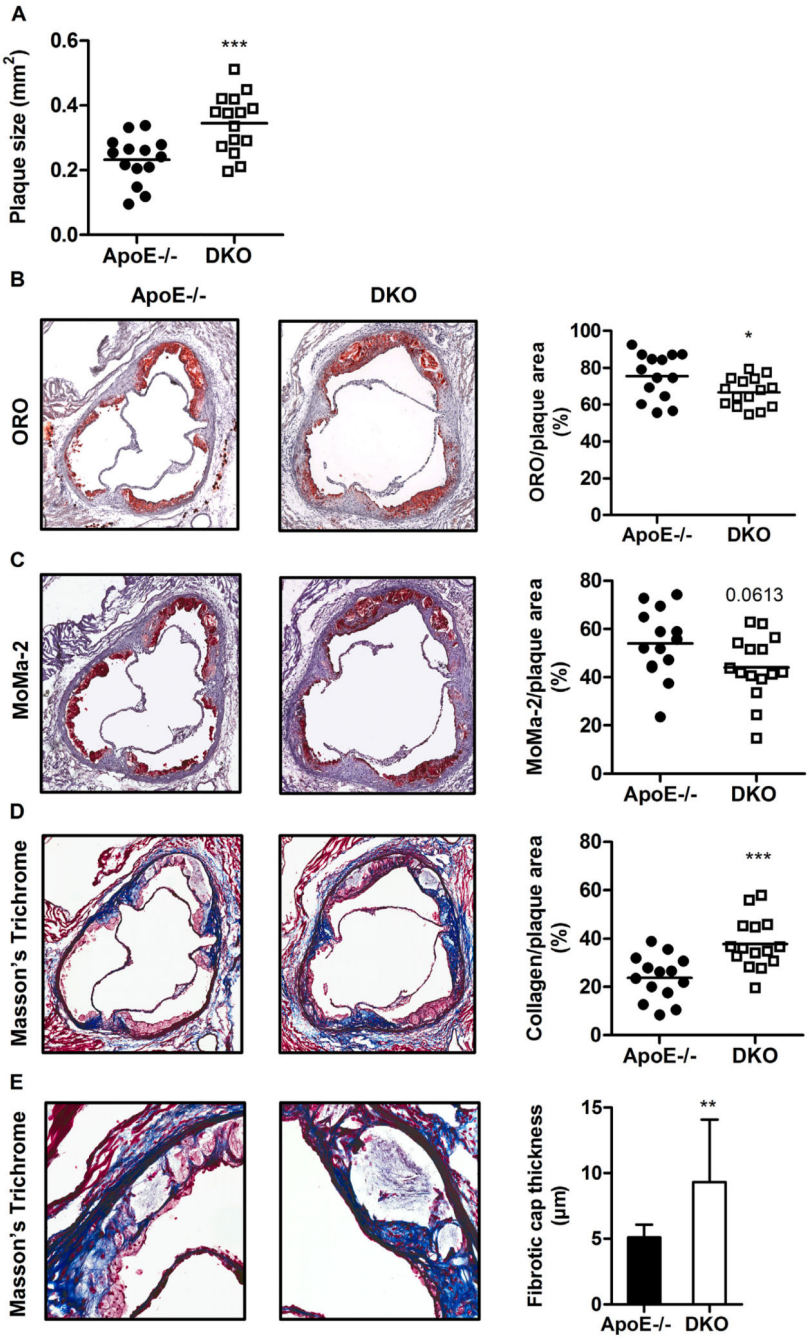

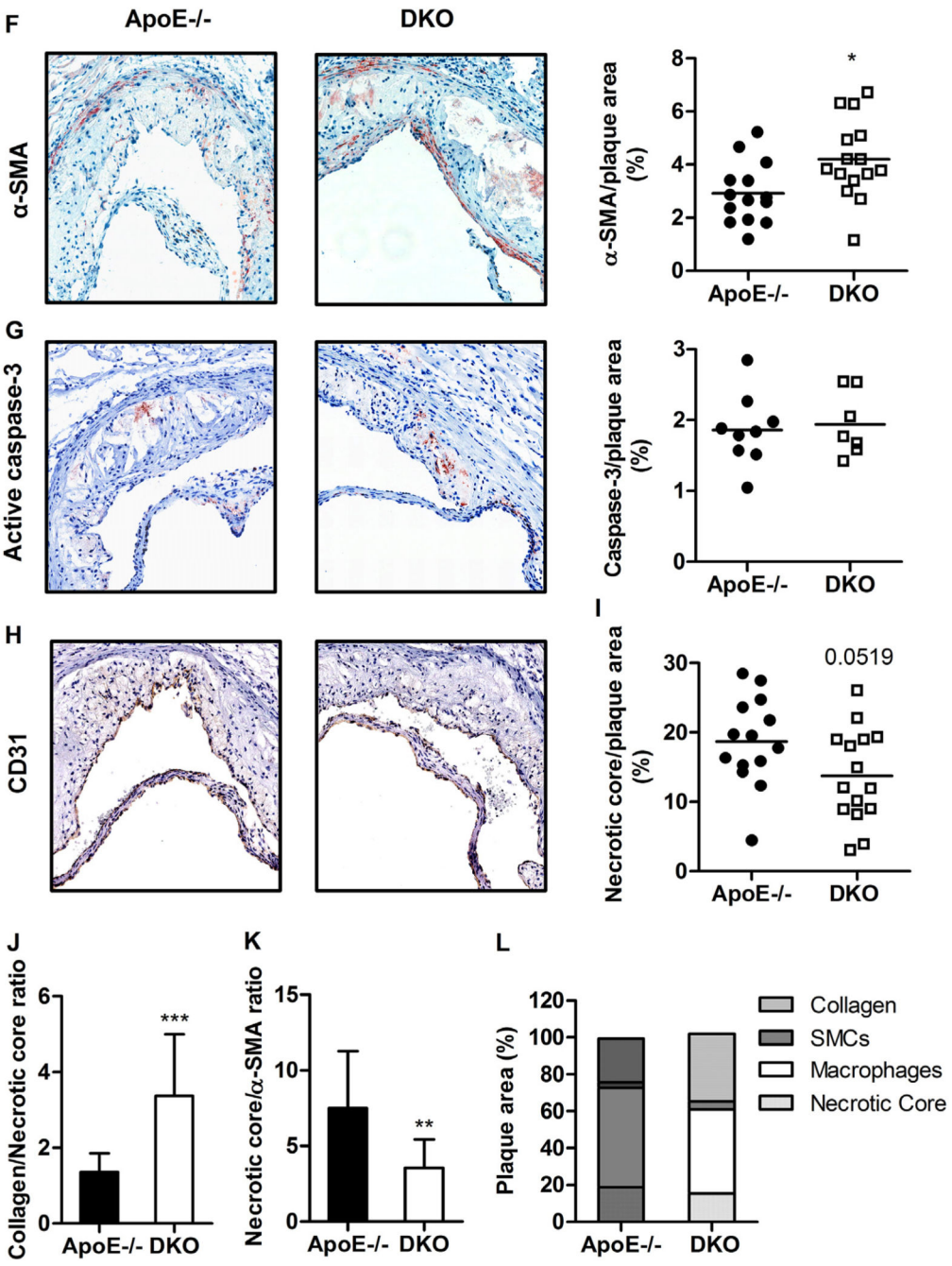

Fig. 6.

Atherosclerotic plaques are more stable in DKO mice. (A) Total lesion size measurements, (B) Oil red O (ORO)-stained lipids (magnification: 5×), (C) MoMa-2 immunohistochemically-stained macrophages (red) (magnification: 5×), (D) Masson's Trichrome-stained collagen (blue) (magnification: 5×), (E) fibrotic cap thickness (n = 14–15) (magnification: 20×), (F) α-smooth muscle actin (α-SMA) immunohistochemically-stained smooth muscle cells (red) (magnification: 15×), (G) active caspase-3 immunohistochemically-stained apoptotic cells (red) (magnification: 15×), and (H) CD31

immunohistochemically-stained neovessels (brown) (magnification: 15×). Data represent mean values of 15 aortic valve sections for lesion size measurements and 3 aortic valve sections in the area of maximal plaque size for ORO, MoMa-2, Trichrome, α-SMA, active caspase-3, and CD31 for each mouse. Bars represent means. Quantification of (I) necrotic core per plaque area, (J) collagen per necrotic area (n = 14–15), and (K) necrotic per α-SMA area (n = 14–15). Data represent means + SD. (L) Distribution of necrotic core, macrophages, smooth muscle cells, and collagen within the plaque. Data represent means (n = 14–15) + SD. *, $p < 0.05$; **, $p \leq 0.01$; ***, $p \leq 0.001$.

Europe PMC Funders Author Manuscripts

Europe PMC Funders Author Manuscripts

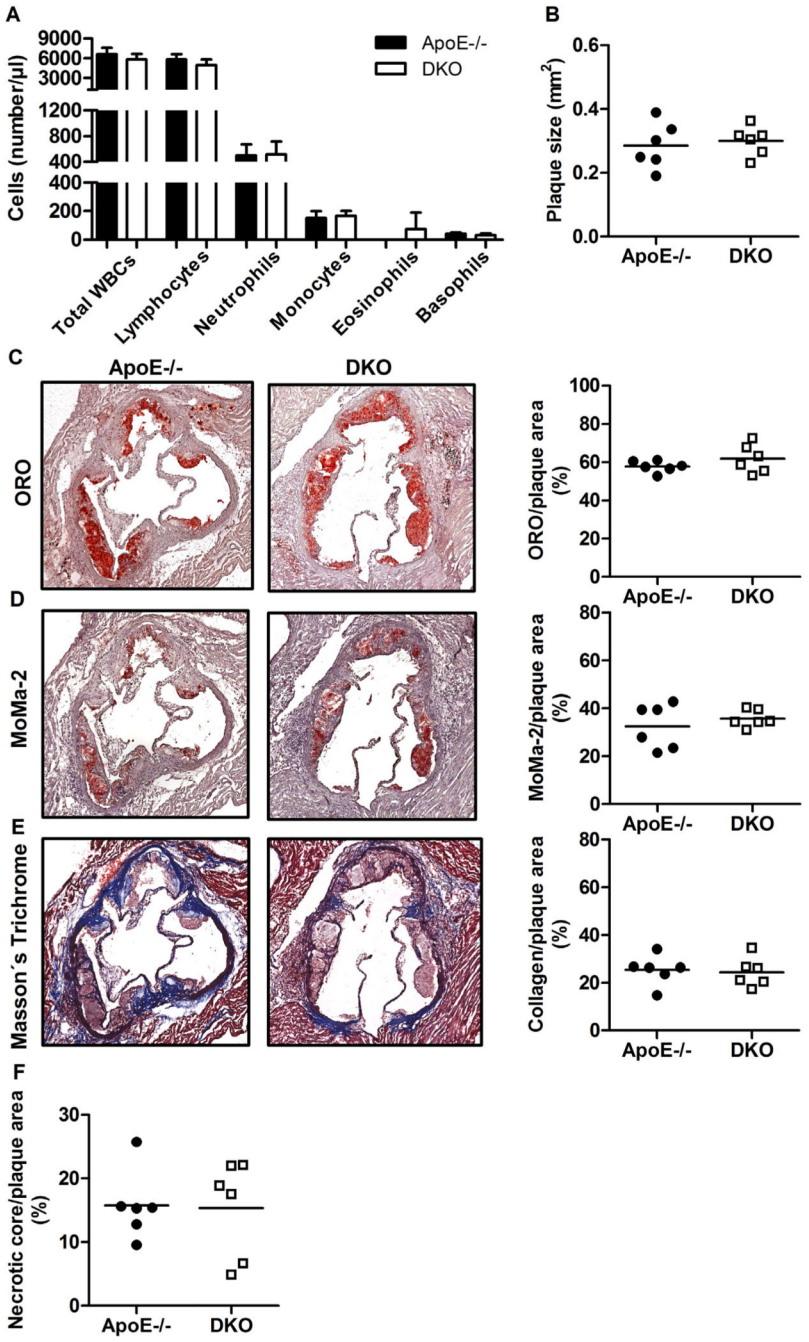

Fig. 7.

CB2R antagonism reverses plaque phenotype in DKO mice. (A) Absolute WBCs after three weeks of SR144528 treatment as means (n = 6) + SD. (B) Total lesion size measurements, (C) Oil red O (ORO)-stained lipids (magnification: 5×), (D) MoMa-2 immunohistochemically-stained macrophages (red) (magnification: 5×), (E) Masson's Trichrome-stained collagen (blue) (magnification: 5×), and (F) necrotic core per plaque area. Data represent mean values of 15 aortic valve sections for lesion size measurements and 3

aortic valve sections in the area of maximal plaque size for ORO, MoMa-2, Trichrome, and necrotic core for each mouse. Data represent means (n = 6) + SD.

Europe PMC Funders Author Manuscripts

Europe PMC Funders Author Manuscripts

Table 1

Plasma parameters of 12 h-fasted ApoE−/− and DKO mice before and after WTD feeding for 8 weeks. Data represent mean (n = 13–14) ± SD.

	Chow diet		Western-type diet (WTD)	
	ApoE−/−	**DKO**	**ApoE−/−**	**DKO**
Triglyceride (mg/dl)	91.2 ± 15.5	92.6 ± 24.6	74.1 ± 15.3	76.5 ± 15.1
Total cholesterol (mg/dl)	224 ± 50.0	249 ± 40.9	1075 ± 167	1160 ± 173
Free cholesterol (mg/dl)	82.6 ± 20.1	91.6 ± 18.5	349 ± 26.9	356 ± 61.4
Cholesteryl ester (mg/dl)	141 ± 33.6	157 ± 26.9	726 ± 156	812 ± 134